Received: 15 July 2020 | Revised: 24 November 2020 | Accepted: 25 November 2020

DOI: 10.1002/term.3164

WILEY

RESEARCH ARTICLE

Cerebrospinal fluid replacement solutions promote neuroglia migratory behaviors and spinal explant outgrowth in microfluidic culture

Richard N. Cliver[1] | Brian Ayers[1] | Alyssa Brady[2] | Bonnie L. Firestein[3] | Maribel Vazquez[1]

[1]Department of Biomedical Engineering, Rutgers, The State University of New Jersey, Piscataway, New Jersey, USA

[2]Department of Physics, Salisbury University, Salisbury, Maryland, USA

[3]Department of Cell Biology and Neuroscience, Rutgers, The State University of New Jersey, Piscataway, New Jersey, USA

Correspondence
Maribel Vazquez, Department of Biomedical Engineering, Rutgers University, The State University of New Jersey, 599 Taylor Road, BME-219, Piscataway, NJ 08854, USA.
Email: Maribel.vazquez@rutgers.edu

Funding information
National Science Foundation, Grant/Award Numbers: CBET 0939511, CBET 1950509; New Jersey Commission on Spinal Cord Research, Grant/Award Numbers: CSCR14IRG005, CSCR17ERG005

Abstract

Disorders of the nervous system (NS) impact millions of adults, worldwide, as a consequence of traumatic injury, genetic illness, or chronic health conditions. Contemporary studies have begun to incorporate neuroglia into emerging NS therapies to harness the regenerative potential of glial-mediated synapses in the brain and spinal cord. However, the role of cerebrospinal fluid (CSF) that surrounds neuroglia and interfaces with their associated synapses remains only partially explored. The flow of CSF within subarachnoid spaces (SAS) circulates essential polypeptides, metabolites, and growth factors that directly impact neural response and recovery via signaling with healthy glia. Despite the availability of artificial CSF solutions used in neurosurgery and NS treatments, tissue engineering projects continue to use cell culture media, such as Neurobasal (NB) and Dulbecco's Modified Eagle Medium (DMEM), for development and characterization of many transplantable cells, matrixes, and integrated cellular systems. The current study examined in vitro behaviors of glial Schwann cells (ShC) and spinal cord explants (SCE) within a CSF replacement solution, Elliott's B Solution (EBS), used widely in the treatment of NS disorders. Our tests used EBS to create defined chemical microenvironments of extracellular factors within a glial line (gLL) microfluidic device, previously described by our group. The gLL is comparable in scale to the in vivo SAS that envelopes endogenous CSF and enables molecular transport via mechanisms of convective diffusion. Our results illustrate that EBS solutions facilitate ShC survival, morphology, and proliferation similar to those measured in traditional DMEM, and additionally support glial chemotactic behaviors in response to brain-derived growth factor (BDNF). Our data indicates that ShC undergo significant chemotaxis toward high and low concentration gradients of BDNF with statistical differences between gradients formed within diluents of EBS and DMEM solutions. Moreover, SCE cultured with EBS solutions facilitated measurement of neurite explant extension commensurate with reported in vivo measurements. This data highlights the translational significance and advantages of incorporating CSF replacement fluids to interrogate cellular behaviors and advance regenerative NS therapies.

KEYWORDS
brain-derived growth factor, chemotaxis, convective-diffusion, Elliott's B solution, Schwann cells

1 | INTRODUCTION

Neurological and neuromuscular dysfunction affect millions of adults, worldwide, as a result of chronic health conditions, genetic disorders, and/or injury to the brain and spinal cord (New et al., 2017). Contemporary studies in the nervous system (NS) have developed spinal explant cultures to examine axonal outgrowth, three-dimensional (3D) tissue organoids to reestablish neuronal synapses, and biomimetic matrixes to aid transplantation of neural stem cells for regeneration (Ichida et al., 2020; Li et al., 2020; Thomson, Hunter, Griffiths, Edgar, & McCulloch, 2006). Recent projects have begun to incorporate neuroglia into these bioengineering systems to leverage glial regenerative abilities to transdifferentiate, migrate to sites of injury, and bridge with adjacent neurons for synaptic function (Jessen et al., 2016; Sohn, Jo, & Park, 2019). Moreover, a growing community has sought to restore NS function via glial-mediated plasticity of synapses, including astrocyte-neuronal synapses in the brain and the tripartite neuromuscular junction (NMJ) for muscle contraction (Flores-Munoz et al., 2020; Natarajan, Sethumadhavan, & Krishnan, 2019). These glial-centric studies have produced genetic models to evaluate glial stem-like properties, microfluidics to interrogate heterogeneous glial-cell interactions, and transplantable nerve grafts to increase synaptic communication (Ottoboni, von Wunster, & Martino, 2020; Singh et al., 2019). Surprisingly, however, the role of cerebrospinal fluid (CSF) that surrounds neuroglia and interfaces with their associated synapses remains only partially explored.

CSF is a complex solution that fills and surrounds the brain ventricular system, its adjacent visual and olfactory cavities, and the central canal and pia mater of the spinal cord. The circulation of CSF around the brain and spinal cord creates microfluidic environments that aid neural response via direct cellular contact with diverse groups of glia (e.g., astrocytes, Schwann, Muller cells), neurons, ependymal, and meningothelial cells (Leister et al., 2020). CSF signaling has become highly significant to regenerative medicine through its regulation of the neurogenic niche, which modulates precursor differentiation, proliferation, and migration (Hashemi et al., 2017; Kaneko et al., 2018). Flow of CSF circulates essential polypeptides, metabolites, growth factors, and other agents that interact directly with glia through the subarachnoid spaces (SAS) of the brain and spinal cord. In vitro studies have demonstrated significant differences in the morphology, growth, and secretions of glia cultured in CSF from injured and damaged animal models. CSF from rats with amyotrophic lateral sclerosis (ALS) initiate profound cellular changes in glia to cause synaptic dysfunction (Shanmukha, Narayanappa, Nalini, Alladi, & Raju, 2018), while CSF from conditions of sepsis and meningitis directly infect glia to influence muscle contraction (Delbaz et al., 2020). Moreover, in vivo rat models of spinal cord injury have used healthy CSF to increase neuronal extension and recovery via collagen nerve guide channels (Farjah, Dolatkhah, Pourheidar, & Heshmatian, 2017). Nonetheless, the vast majority of tissue engineering studies continue to use conventional cell culture media, such as Neurobasal (NB) and Dulbecco's Modified Eagle Medium (DMEM), in the study of neural stem cells, transplantable biomaterials, and development of organotypic explants that model spinal injury and disease (Cembran, Bruggeman, Williams, Parish, & Nisbet, 2020; Tsintou, Dalamagkas, & Makris, 2020).

The current project examined in vitro behaviors of glial Schwann cells (ShC) and spinal cord explants (SCE) within extracellular environments of a CSF replacement fluid, Elliott's B Solution (EBS), compared against traditional DMEM and NB media. These studies were performed within a microfluidic device previously developed by our laboratory, called the glial line (gLL) (Pena, Robles, Zhang, & Vazquez, 2019), designed to mimic the micrometer scale of the SAS and the mechanisms of transport occurring therein. EBS is an FDA-approved solution comparable to healthy CSF in pH, electrolyte composition, glucose content, and osmolality (Shimada et al., 2020; Stark, Josephs, Dulak, Clague, & Sadiq, 2019). EBS is most clinically used as a diluent of therapeutics for disorders of the meninges, which partially contain CSF and have been implicated in neuromuscular disease, neurodegenerative disorders, and some forms of cancer (Oka, Yamamoto, Nonaka, & Tomonaga, 1996; Shestakova, Healey, Zhao, Rezk, & Nakagiri, 2019). Results of our study illustrate that EBS solutions facilitate ShC survival, morphology, and proliferation similar to those measured in traditional DMEM medium, and additionally support glial chemotactic behaviors in response to the regenerative agent, brain-derived growth factor (BDNF) (Singh, Robles, & Vazquez, 2020). Moreover, SCE cultured with EBS solutions exhibited survival rates comparable to those within conventional NB medium, and demonstrated rates of cellular outgrowth commensurate with reported in vivo measurements. These data highlight the translational significance of creating clinical microenvironments of CSF with appropriate anatomical scale to examine cellular behaviors. Our results point to the underexplored advantages of incorporating CSF replacement fluids in tissue engineering studies of neuro-regeneration using microfluidic environments.

2 | METHODS AND MATERIALS

2.1 | Cell culture

ShC were modeled using an immortalized cell line (S42; ATCC, CRL-2942) and were thawed from aliquots stored in nitrogen tanks, plated onto sterile, tissue culture flasks, and cultured using sterile DMEM (ATCC, Cat. No. 30–2002) containing 10% fetal bovine serum

Components	DMEM	NB	EBS	CSF	Notes
Inorganic salts	+	+	+	+	$CaCl_2$, KCl, NaCl, etc.
Amino acids	+	+	−	−*	L-Arg, L-Cys, L-Leu, L-Met, L-Trp, L-Val, etc.
Vitamins	+	+	−	−	B-9, B-3, B-2, etc.
Other	+	+	−	−*	Phenol red, Sodium Pyruvate, HEPES
D-glucose	+	+	+	+	DMEM/NB: 4.5 g/L
					EBS: 0.8 g/L
					In vivo: 0.6 g/L
Osmolarity	290	260	288	295	Measured in mOsm/L
pH	7.4	7.25	6.0–7.5	7.31	

*The asterisk (*) denotes that only trace amounts of amino acids and vitamins are found within in vivo CSF.

TABLE 1 Comparison of the primary chemical constituents within extracellular solutions of Dulbecco's Modified Eagle Medium (DMEM), Neurobasal (NB) medium, Elliott's B Solution (EBS), and in vivo cerebrospinal fluid (CSF)

(FBS) and 1% penicillin–streptomycin (Gibco, Cat. No. 15070063). ShC culture flasks were previously treated with 15 ug/ml of poly-L-lysine (Sigma-Aldrich, Cat. No. P-9155) for at least 2 h at 37°C, as per convention (Pena et al., 2019). The flasks were prepared by aspirating the poly-L-lysine solution, rinsing once with deionized phosphate-buffered saline (PBS), and air-drying, uncapped, in an upright position in a biological cabinet for 30 min prior to use. All cells were cultured at 37°C, 95% humidity, and 5% CO_2 and passaged at 80%–90% confluency. To dislodge cells from the flask, cultures were incubated in accutase (ICT, Inc., San Diego, Cat. No. AT104-500) for 5 min at 37°C and centrifuged at 1500 rpm for 3 min. Cell medium was replaced every 2 days, and cultures were allowed to reach 80%–90% confluency before harvesting for testing. S42 cells have been used to model the behaviors of ShC by our group Pena et al. (2019) and others (Castelnovo et al., 2020; Lackington, Raftery, & O'Brien, 2018; Sasagasako, Toda, Hollis, & Quarles, 1996) because the cultured cells have been shown to, both, resemble ShC at an early stage prior to myelination Toda, Small, Goda, and Quarles (1994) and illustrate consistent cell behavior in vitro. Our current study continued to use S42 as models for ShC for continuity with our previous work and maintained doubling times and seeding densities that were appropriate for comparison across studies.

2.2 | Reagents

Cultures were performed using three media solutions: DMEM, NB medium, and EBS, all with 10% FBS and 1% penicillin-streptomycin. ShC cultures were performed using two media solutions of DMEM and EBS, all with 10% FBS and 1% penicillin-streptomycin, as per convention (Pena et al., 2019; Shen, Tang, Cao, Cao, & Ding, 2017). Explant cultures were performed in solutions of NB Media and EBS solutions supplemented with B27 and 0.5 mM Glutamax as per convention so as to provide long-term viability to maturing neurons (Brewer, Torricelli, Evege, & Price, 1993; Chen et al., 2010; Thomson et al., 2008). We note that control experiments cultured explants in DMEM to report poor viability, no robust outgrowth, and minimal neurite extension as per the literature (Thomson et al., 2006). (data not shown.) All media types contain inorganic salts, vitamins, amino acids, and glucose in varying concentrations as per Table 1. EBS was purchased in 10 ml ampules (Lukare Medical LLC, NJ; NDC 55792-07-01) that were filtered to remove any particulates prior to use. In addition, controlled concentrations of brain-derived neurotrophic factor (BDNF: 100 ng/ml, Cat. No. 248-BD-005, R&D Systems) were used to develop extracellular gradients for testing. CellTracker™ Green CMFDA Dye was used for the staining and measurements of explants (ThermoFisher Scientific, Cat. No. C2925).

2.3 | Glia line microfluidic system

This project adapted a modified glia line (gLL) microfluidic system, previously described by our group (Pena et al., 2019), to examine glial migratory behaviors. The device is manufactured from elastomeric polydimethylsiloxane (PDMS: Sylgard 184, Dow Corning) bonded onto a glass slide chemically cleaned with commercial piranha solution (Nanostrip, VWR). The system is comprised of two layers as shown in Figure 1. The top layer contains two large volume chambers, labeled cell chamber and source chamber, and are both 3-mm tall with a radius of 6-mm. They are connected by a so-called bridge channel 7.5-mm long, 2.5-mm tall, and 4-mm wide to make fluidic contact between the chambers. Both chambers are also in fluidic contact with the bottom layer of the device, which contains two 6.3-µl reservoirs which are 4-mm tall and 1-mm in diameter, labeled cell and source reservoir, connected by a microchannel. The channel is of 12-mm length and 250-µm hydraulic diameter, as per Figure 1. Devices were fabricated by using a 9:1 pre polymer mixture of PDMS that was thoroughly mixed, vacuum desiccated, and poured onto a computer numerical control (CNC)-milled, aluminum mold created with micrometer features. The PDMS was allowed to polymerize in a convection oven at 105°C for 30 min and then bonded onto cleaned microscope glass slides using corona plasma treatment to create a closed system. The glia line microfluidic device (gLL) system provides a microchannel that is readily micro-manufactured and modified as

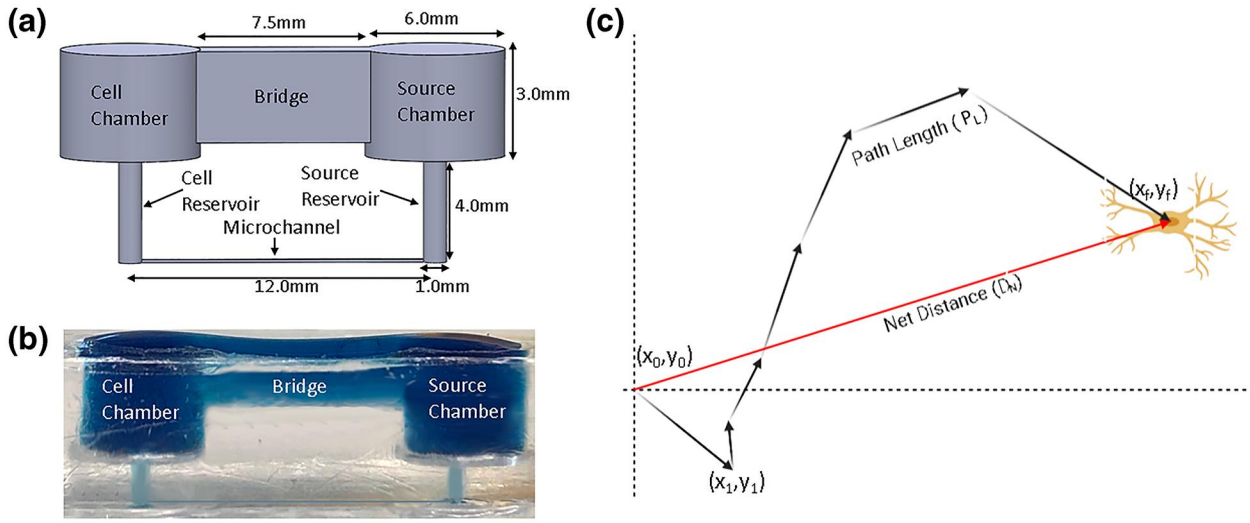

FIGURE 1 Description of the bridged glia line (gLL) microfluidic system used to produce chemically controlled, extracellular environments for testing. (a) Schematic of the bridged gLL system comprised of two large cell and source chambers of 330 μl connected by a bridge channel. The chambers are fluidically connected to smaller reservoirs of 6.3 μl directly beneath each, denoted as cell and source reservoirs, respectively. These μl-reservoirs are additionally connected to one another via a channel of 250-μm diameter, wherein cell responses are measured. (b) Image of the bridged gLL system fabricated using transparent PDMS, where fluidic spaces are filled with blue dye for visualization. (c) Rendering of a representative cell trajectory within the gLL microfluidic channel to illustrate measurement of cell path length, PL, and net distance traveled, DN, per spatial position (*x*,*y*) [Colour figure can be viewed at wileyonlinelibrary.com]

needed. Motivations for the use of the gLL in this study include an equivalently sized system of the in vivo SAS where CSF resides, and a bridge reservoir system (Figure 1a) to enable transport via convective-diffusion (CD), as per recent models of the in vivo flow of CSF within the SAS (Thomas, 2019). CD is a transport mechanism most commonly applied in the analysis of interstitial flows, such as in the cardiovascular, renal, and NSs, among others (Sun et al., 2014). Here, transport occurs via a combination of molecular diffusion and convection induced by bulk fluid velocity as shown in Equation 2. The gLL was used to measure cell migratory behavior, and as such, chemotaxis experiments were preformed prior to S42 proliferation in the microchannels (Pena et al., 2019).

The gLL operates by inserting a brain-derived neurotrophic factor (BDNF) ligand solution into one reservoir (source) and a cell buffer solution in the opposite reservoir (sink). In the absence of bulk flow, transport along the adjoining microchannel between reservoirs is then generated by Fick's law of one-dimensional diffusion, shown in Equation (1). When a small bulk flow is added, transport is governed by (CD), described by Equation (2).

$$\frac{\partial C}{\partial t} = D_i \frac{\partial^2 C_i}{\partial x^2} \tag{1}$$

$$\frac{\partial C}{\partial t} = D_i \frac{\partial^2 C_i}{\partial x^2} + v_B \frac{\partial C_i}{\partial x} \tag{2}$$

where C_i represents ligand concentration in ng/ml, t is time measured in seconds, D_i denotes molecular diffusivity in m^2/s, and V_B is bulk flow in m/s. The chemical distribution of the ligand within the modified gLL microchannel was solved analytically for both cases and experimentally verified to within 2% error (Pena et al., 2019). The diffusion coefficient, D_i, of BDNF was estimated as 1.4×10^{-6} cm^2/s, using its Stokes radius and molecular weight, as well as experimentally measured data in the published literature. The diffusivity predicts that a steady-state concentration gradient of BDNF is generated within the microfluidic system after approximately 18 h. Transport via CD facilitates a spatiotemporal evolution of a steady-state BDNF gradient in the gLL microfluidic system. The steady-state BDNF concentration profile is highly nonlinear, as shown in Figure 3a, and is achieved at approximately 18 h in our experiments. All data was collected in response to this BDNF steady-state profile, which was maintained in the gLL system for several days. A sample of 12–15 cells were measured per gradient region of the gLL device in triplicate for all experiments.

Inner substrate surfaces of modified gLL devices were coated with laminin (LM: Thermo Fisher, Cat. No. 23017015) prior to all testing. Approximately 150 μl of LM (15 μg/ml) was manually inserted into the source reservoir of the gLL system using a 1-ml syringe (BD Biosciences, Cat. No. 309,659) and incubated at 37°C in a 5% CO_2 incubator for 1 h to facilitate cross-linking of laminin subunits. The gLL was then rinsed with PBS (Gibco, Cat. No. 10010023) prior to insertion of cells.

2.4 | Computational transport model and experimental validation

A one-dimensional numerical simulation of molecular transport within the gLL system was performed using COMSOL Multiphysics (Version 5.3a, Stockholm, Sweden). Mathematical computation determined the concentration profile using Equations (1) and (2) for

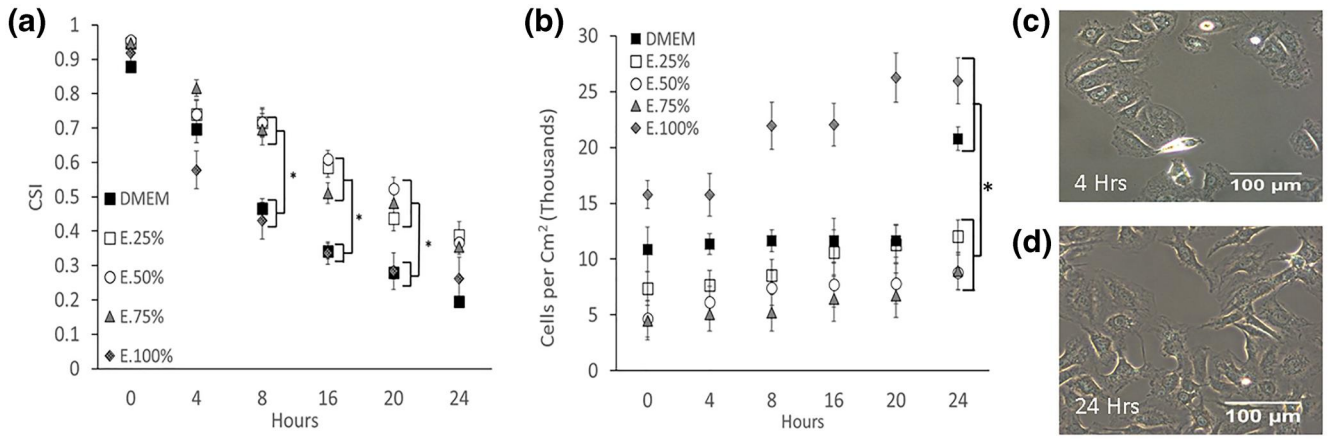

FIGURE 2 Schwann cell (ShC) morphology and proliferation rates over time in solutions of Dulbecco's Modified Eagle Medium (DMEM) and DMEM-titrated solutions of Elliott's B solution (EBS). Note that all solutions were prepared with fetal bovine serum (FBS) and penicillin-streptomycin to maintain in vitro cell survival. (a) Changes in ShC morphology measured via cell shape index (CSI) in DMEM titrated solutions of 25%, 50%, 75%, and 100% EBS alongside CSI measurements of ShC in 100% DMEM solutions (control). A cell sample of $n = (30–35)$ cells was used per experimental time point shown. (b) Proliferation rates of ShC in DMEM-titrated solutions of EBS and 100% DMEM solutions (control). A sample of $n > 2000$ cells was used per experimental condition, in triplicate. (c) Representative image of ShC after 4 h of culture in 100% EBS solution and (D) after 24 h in culture in 100% DMEM (scale = 100 µm). Statistical significance of $p < 0.05$ is denoted with an asterisk (*) while significance of $p < 0.01$ is represented by a double asterisk (**) [Colour figure can be viewed at wileyonlinelibrary.com]

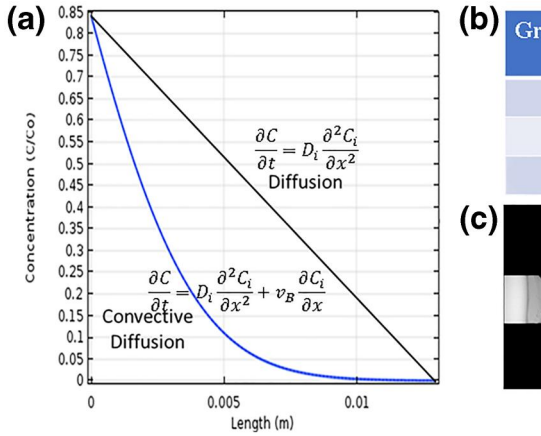

(b)

Gradient	Range (ng/mL per mm)	Average (ng/mL per mm)	Length (mm)
G_H	0.853 – 0.194	0.472	0-4
G_M	0.194 – 0.02	0.076	4-8
G_L	0.02 – 0.001	0.008	8-12

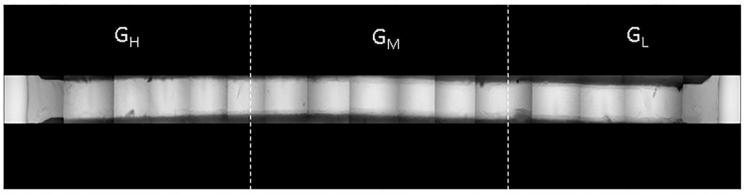

FIGURE 3 Summary of chemical microenvironments produced within the bridged glia line (gLL) microfluidic system. (a) A normalized, nonlinear concentration of BDNF against microchannel position (x, y) is plotted in steady-state when transport is governed by convective-diffusive (CD) transport. This is compared against the linear, steady-state concentration profile of BDNF along the microchannel length developed via diffusive transport, alone. (b) Quantitative distribution of BDNF concentration along the gLL microchannel length as within different channel lengths that represent high (G_H), medium (G_M), and low (G_L) concentration gradient. (c) Representative images of CD transport of a model BDNF fluorescent molecule (MW = 13.5 kDa) in the gLL system at steady-state (shown in white) [Colour figure can be viewed at wileyonlinelibrary.com]

diffusion. Analysis was performed at steady state using laminar and incompressible flow ($\rho = 1070$ kg/m^3) at constant viscosity ($\mu = 1.05$ Pa-s). Boundary conditions used no slip at the inner surface walls and axial symmetry within the microchannels, while gravity effects were presumed to be negligible. An inlet concentration of $C_o = 100$ ng/ml of BDNF was used to approach the in vivo values cited in the literature (Singh et al., 2020). Experiments used a model fluorescent molecule of comparable molecular weight (FITC-Dextran, CAS 60842-46-8 [20 kDa], Sigma-Aldrich, St. Louis, MO) to validate the concentration distributions predicted by the computational model within the gLL. The resulting values of fluorescence intensity, I, along the microchannel length were measured via microscopy to estimate the changes in concentration, C, within the device.

2.5 | Measurement of cell viability, proliferation, morphology, and migration

ShC were seeded and left to attach for 24 h in LM-coated devices. Representative cell groups were analyzed after 24 h, and a ratio of

live to dead cells was established to estimate viability upon the different substrate platforms. Viability was calculated via a parameter of survival, S, that used optical assessment of cellular attachment and cell-body size upon substrate adhesion to denote cell detachment as death. Our data illustrates extremely high viability in vitro (greater than 95%) over the time course of experiments, which support results of our previous studies using these ShC models and quantitative assays (Pena et al., 2019). Proliferation was measured using direct cell counting. The morphology of ShC was evaluated using the Cell Shape Index (CSI), a dimensionless parameter widely used to quantify the roundness of a cell and defined in Equation (3):

$$\mathrm{CSI} = \frac{4\pi A_S}{P^2} \tag{3}$$

where, A_S is the cell surface area (μm^2) and P (μm) is the perimeter of the cell. The value of the CSI ranges from 0 to 1, where values close to 1 represent a perfectly rounded cell and values approaching 0 denote a purely bipolar and elongated cell (Pena et al., 2019). All measurements were performed using DMEM-titrated EBS solutions from E25% to E100%. In this nomenclature, E25% refers to a solution that is comprised of 25% EBS and 75% DMEM whereas E50% denotes a solution comprised of 50% EBS and 50% DMEM. In addition, all solutions were constituted using 10% FBS and 1% penicillin-streptomycin. Further, a solution of 100% DMEM was used as the control solution for all experiments. Finally, migration was evaluated by the use of net distance (D_N) and path length (P_L), defined in Equations (4) and (5), respectively, and found in Figure 1c.

$$D_N = \sqrt{|(y_f - y_0)|^2 + |(x_f - x_0)|^2} \tag{4}$$

where coordinates (x_0,y_0) are used to denote the initial position of motile cells and (x_f,y_f) denote the final position of motile cells.

$$P_L = \sum_{n=1}^{i} \sqrt{(y_n - y_{n-1})^2 + (x_n - x_{n-1})^2} \tag{5}$$

where coordinates (x_n,y_n) and (x_{n-1},y_{n-1}) are used to denote the summation of all cell displacements from an initial position (x_0,y_0) to a final position (x_f,y_f).

2.6 | Organotypic cultures of spinal cord explants

All animal studies were performed in accordance with US Department of Health and Human Services Guide for the Care and Use of Laboratory Animals and were approved by the Rutgers University Institutional Animal Care and Use Committee (IACUC Proto #00-010). SCE were obtained from Sprague Dawley rat pups (E18), as previously described (Avossa, Rosato-Siri, Mazzarol, & Ballerini, 2003). Briefly, pregnant mice were sacrificed by CO_2 overdose and fetuses delivered by cesarean section. Embryos were decapitated with forceps, a dorsal incision was made along the midline of the body from cephalad to caudal to a depth just superficial to the spinal cord, and spinal cords were extracted by their lumbar, and if necessary, cervical ends. Spinal cords were then transversely sliced (275 μm) with a tissue chopper (McIlwain Tissue Chopper, IL). All efforts were made to minimize animal suffering and reduce numbers of animals used. A total of eight mice were sacrificed and three to five spinal explants per mouse were used to gather data per experimental condition.

2.7 | Imaging and analysis

An inverted epi-fluorescence microscope (Leica DMI8) was used to observe cell behavior over time and to perform optical analysis with a cooled CCD camera (DFC7000 GT, Leica Microsystems, Wetzlar, Germany) using a 20× magnification (DMi8 Leica Microsystems Inc., IL). To hold the bonded glass slides, an insertable frame was used (H301-K-FRAME, Leica). Microscope images were gathered for fluorescent dextran using ImageJ (Pena et al., 2019) to determine intensity values (8 bit scale: 1–255) over position and time. Migration mapping was performed using ImageJ. A cell sample of 12–15 cells was selected from each gradient region of the device, and the cell centroid computationally tracked over the time points. SEM was calculated for Figure 4a–c by averaging the net distance of each point of five motile ShC cells, taking the SD, dividing by the total number of points, and multiplying by the pixel-to-micron conversion factor for a 20× image. SCE measurements were performed by staining the explant with CellTracker™ Green. Explant measurement were performed using the established, rectangular fit method (Haines et al., 2010) to determine explant diameters, d_1 and d_2, and their respective averages.

2.8 | Statistical analysis

One-way ANOVA was used to analyze statistical significance among all experimental groups. Each dataset was gathered from a minimum of $n = 15$ cells per region per device, in triplicate. Values are reported using mean and SE. The post-hoc Tukey test was used to determine levels of significance between experimental groups and control, where p-values < 0.05 were denoted by an * and $p < 0.01$ were marked with **.

3 | RESULTS

3.1 | Schwann cell morphology and proliferation in extracellular solutions

Differences in ShC morphology and proliferation rates were examined over time when cultured in extracellular solutions produced using titrated amounts of 25%, 50%, 75%, and 100% of EBS solution and conventional DMEM medium (all with FBS). ShC in DMEM

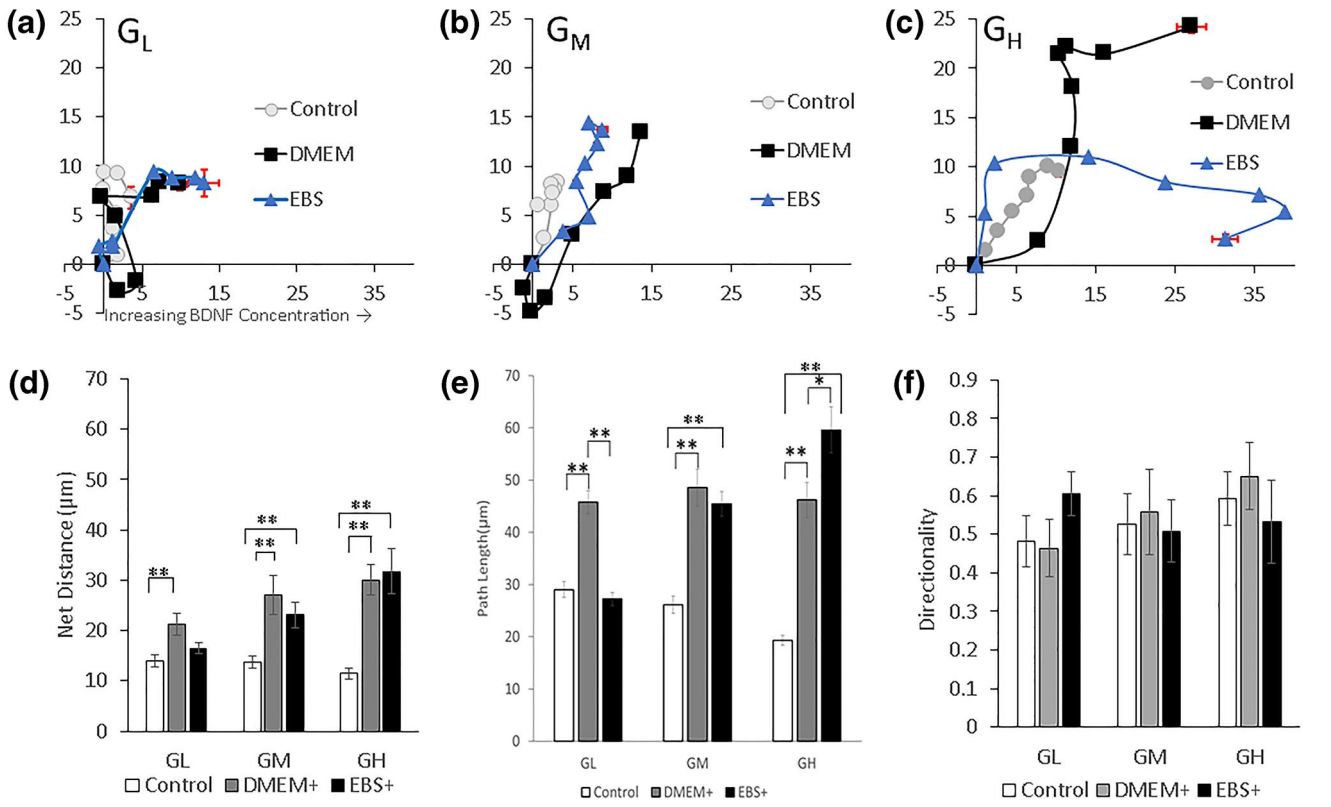

FIGURE 4 Migration of Schwann cells (ShC) toward microfluidically-controlled gradients of Brain-Derived Neurotrophic Factor (BDNF) produced within solutions of Dulbecco's Modified Eagle Medium (DMEM) and Elliott's B solution (EBS). Trajectories of motile ShC within the gLL microfluidic system containing (a) low BDNF gradients, G_L, (b) medium BDNF gradients, G_M, and (c) high BDNF gradients, G_H, produced within solutions of DMEM and EBS. Control tests measured ShC migration in DMEM solutions, only, without BDNF. Each trajectory represents an average of five motile ShC per test condition. Error bars are illustrated by averaging the five motile ShC, taking the Standard Error of the Mean (SEM), and applying to the final position. (d) Average net distances, DN, traveled by ShC towards increasing BDNF gradients produced within EBS and DMEM solutions. (e) Average path lengths, PL, of ShC toward BDNF gradients produced within EBS and DMEM solutions. A cell sample of $n = (12–15)$ cells was measured per gradient region of the gLL device in triplicate. Statistical significance of $p < 0.05$ is denoted with an asterisk (*) while significance of $p < 0.01$ is represented by a double asterisk (**) [Colour figure can be viewed at wileyonlinelibrary.com]

solutions (used as control) exhibited increasingly elongated morphology over time, with values of CSI decreasing from a high of 0.85 (i.e. highly rounded) to 0.25 (more elongated) over 24 h, as shown in Figure 2a. Similarly, the CSI values of ShC in 100% EBS solution (denoted as CSI^{100}) decreased from $0.95 < CSI^{100} < 0.35$ during the same 24-h period. CSI values of ShC within titrated amounts of EBS solutions illustrated slower rates of elongation with average values between $0.92 < CSI^{75} < 0.35$ for 75% titrated solutions, $0.96 < CSI^{50} < 0.36$ for 50% titrated solutions, and $0.97 < CSI^{25} < 0.38$ for 25% titrated EBS solutions. Proliferation of ShC was also measured in titrated solutions of EBS and DMEM media (all with FBS). As shown in Figure 2b, ShC in 100% EBS proliferated from 2E4 cells per cm^2 at time $t = 0$ to 3.5E4 per cm^2 at $t = 24$ h, a 57% increase. ShC in 100% DMEM proliferated from 1E4 per cm^2 to 2.2E4 per cm^2 during that same time period, for an increase of 45%. ShC proliferation was slower in lower titrated solutions of 75%, 50%, and 25% EBS with values less than 1.5E4 cells per cm^2 and increases of less than 10% over 24 h, each. Figure 2c,d illustrate the morphology and proliferation of representative ShC after 4 and 24 h of culture in DMEM with FBS, respectively. We note that while cells do not proliferate at identical rates, experiments of this study used doubling times as averages to represent differences in cell proliferation induced by EBS and DMEM solutions. Statistical significance of $p < 0.05$ is denoted with an asterisk (*) while significance of $p < 0.01$ is represented by a double asterisk (**).

3.2 | Extracellular microenvironment

We developed a microfluidic environment to model the SAS of the central NS that creates fluidic contact between cells and circulating CSF. A microsystem previously developed by our group, called the gLL, was modified to include a small convective velocity, V_B, that created a nonlinear concentration profile within the cellular microenvironment. The addition of this bulk flow produced an extracellular chemical environment via CD that was significantly different than that produced via the diffusional processes of Fick's law or convective Poiseuille flow, individually. As shown in Figure 3, transport of biocompounds via CD produced a highly nonlinear gradient profile with varying concentration gradient regions along the axial length of the microchannel. For

ease of analysis, our study defined three separate gradient regions within the microchannel using a normalized concentration gradient of (C/C_o). The portion of the microchannel closest to the chemical source, that is 0 mm < L < 4 mm, maintained a steady-state chemical environment with a normalized concentration range of 0.85 < $^{H}(C/C_o)$ < 0.19. The average concentration gradient, G, within this section was highest, and measured as $G_H = 0.472$ per mm of channel. An average medium concentration gradient of $G_M = 0.076$ was produced within the adjacent channel segment between 4 mm < L < 8 mm, where the normalized concentration range was 0.19 < $^{M}(C/C_o)$ < 0.02. An average low concentration gradient of $G_L = 0.008$ was produced within the final channel section between 8 mm < L < 12 mm, with a normalized concentration range of 0.002 < $^{L}(C/C_o)$ < 0.0001. By contrast, transport via diffusion alone produced a linear concentration gradient of $G_{DIFF} = 0.072$ along the full microchannel length (L = 12 mm). The distribution of each concentration field is summarized in Figure 3b and a representative image used to measure chemical transport in the bridged gLL system is seen in Figure 3c. Statistical significance of $p < 0.05$ is denoted with an asterisk (*) while significance of $p < 0.01$ is represented by a double asterisk (**).

3.3 | Chemotactic migration of Schwann cells

The migratory responses of ShC toward chemical fields created within extracellular solutions of DMEM and EBS were measured using our bridged gLL microfluidic system. Experiments produced controlled concentration gradient fields of BDNF, a well-known chemoattractant of ShC that is often used for neural repair. The trajectory of individual ShC within microfluidic devices was imaged over time to obtain measurements of average ShC path length, PL, and net distance traveled, DN, in low, medium, and high gradient fields of extracellular BNDF. As shown in Figure 4, ShC migrated chemotactically toward increased BDNF gradients produced within both DMEM and EBS solutions and with high statistical significance ($p < 0.01$) compared against control (100% DMEM without BDNF). As shown in Figure 4, ShC migrated chemotactically toward increased BDNF gradients with high statistical significance ($p < 0.01$) when compared to DMEM control (DMEM-BDNF) in both DMEM and EBS solutions. Figure 4a–c illustrate representative trajectories of ShC in response to BDNF gradient fields created within extracellular solutions of EBS and DMEM. As seen, trajectories illustrate similar patterns with some differences in overall values of PL and net distances traveled (defined in Figure 1c). First, the average net distance traveled, that is DN or the shortest distance between a cell's initial and final position in the bridged gLL, was significantly higher ($p < 0.01$) for both DMEM and EBS solutions towards BDNF than in control (no BNDF) at all gradient fields. Second, no statistical significance ($p > 0.05$) was observed in the average net distances of ShC traveled toward BNDF within DMEM or within EBS solutions at any gradient field, G_L, G_M, or G_H, as per Figure 4d. Third, the average PL of motile ShC, that is PL or total distance traveled, was significantly higher in both DMEM and EBS solutions compared to control (no BDNF). Average PLs of ShC toward low BNDF gradients, G_L, were higher in solutions of DMEM ($^{GL}PL_D = 45.763 \pm 2.205$) than EBS ($^{GL}PD_E = 27.226 \pm 1.292$) but were statistically insignificant ($p > 0.5$) toward medium gradients, G_M, generated within each extracellular solution. Average PL of ShC within high BNDF gradients, G_H, were larger in EBS solutions ($^{GH}PL_E = 59.598 \pm 4.413$) than DMEM ($^{GH}PL_D = 46.202 \pm 3.38$), as per Figure 4e. EBS + conditions were calculated in G_H, G_M, and G_L over control and found to be significant at $p < 0.01$, for all regions except G_L. Lastly, no differences were measured in the directionality, D, of ShC towards any gradient field of BDNF produced within extracellular solutions of EBS or DMEM, as shown in Figure 4f. SEM was calculated for Figure 4a–c by averaging the net distance of each point of five motile ShC cells, taking the SD, dividing by the total number of points, and multiplying by the pixel-to-micron conversion factor for a 20× image.

3.4 | Viability and outgrowth of spinal cord explant cultures

Experiments next examined differences in the viability of SCE maintained within extracellular solutions of EBS and NB media. SCE were cultured within conventional 24 well plates for up to 12 days in vitro (DIV). SCE viability was measured as 100% at DIV8 for both EBS and NB solutions, but was reduced to 82% survival in EBS and 87% in NB at DIV12. SCE outgrowth was then estimated within each extracellular solution by measuring average cellular extensions over time. Figure 5 illustrates cellular outgrowth of a representative SCE from day in vitro DIV6, DIV 8, and DIV 10, where cellular extensions are seen to increase over time as measured by the conventional rectangle method using the d1 and d2 axes shown. Data illustrate that SCE outgrowth within NB exhibited an average diameter of $d_{NB} = 1.63 \pm 0.09$ mm at DIV8 while outgrowth within EBS produced a smaller average diameter of $d_{EBS} = 1.23 \pm 0.10$ mm at DIV8.

Follow-up tests then examined changes in SCE outgrowth measured within each extracellular solution of EBS and NB in the presence of extracellular ShC. SCE were cultured in 24 well plates using EBS and NB for up to 10 days with four extracellular ShC conditions: (i) No extracellular ShC (control); (ii) Low density ShC solutions (ρ_L = 1E8 cells/ml); (iii) Medium ShC density (ρ_M = 1E9 cells/ml); and (iv) High ShC density (ρ_H = 1E10 cells/ml).

We observed that SCE in NB without extracellular ShC (control) demonstrated the largest outgrowth with an average diameter of $d_{NB} = 1.69 \pm 0.13$ mm at DIV8. SCE cultured in NB with high ShC density, ρ_H, exhibited an outgrowth with an average diameter of $^{\rho H}d_{NB} = 1.78 \pm 0.04$ mm, while SCE in medium ShC density, ρ_M, exhibited an average diameter of $^{\rho M}d_{NB} = 1.39 \pm 0.27$ mm. SCE cultured in NB with low ShC density, ρ_L, exhibited an average outgrowth diameter of $^{\rho L}d_{NB} = 1.44 \pm 0.35$ mm. As seen in Figure 5d, values of average SCE outgrowth exhibited statistical significance between control and ShC addition ($p < 0.01$), but not across different ShC densities. By contrast, SCE cultured in extracellular solutions of

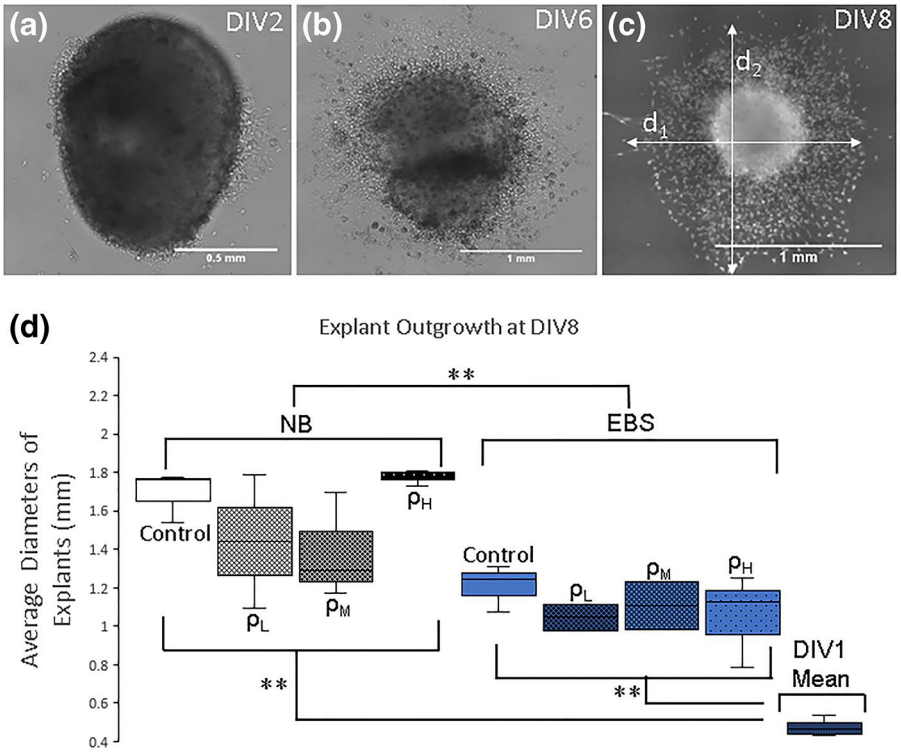

FIGURE 5 Average diameter of spinal cord explants (SCE) after culture of 8 days in vitro (DIV) within extracellular solutions of Neurobasal (NB) media and Elliott's B solution (EBS). (a) Representative SCE at day DIV 2. (b) Images of SCE at DIV 6 and at (c) DIV 8 illustrating outgrowth measurement using the rectangular fit method using d1 and d2 axes, shown. (d) Measurement of SCE outgrowth in NB and EBS solution using a low density of extracellular ShC (ρ_L = 10E8 cells/ml), medium ShC density (ρ_M = 10E9 cells/ml), and high ShC density (ρ_H = 10E10 cells/ml). Statistical significance of $p < 0.05$ is denoted with an asterisk (*) while significance of $p < 0.01$ is represented by a double asterisk (**) [Colour figure can be viewed at wileyonlinelibrary.com]

EBS illustrated small variations in SCE outgrowth diameter via influence of surrounding ShC densities. SCE cultured in EBS without extracellular ShC (control) exhibited average outgrowth diameter of $d_{EBS} = 1.21 \pm 0.12$ mm, while SCE cultured in EBS solutions at high ShC density, ρ_H, demonstrated an average diameter of ${}^{\rho H}d_{EBS} = 1.05 \pm 0.24$ mm. SCE cultured in EBS solution with medium ShC density, ρ_M, illustrated an average outgrowth diameter of ${}^{\rho M}d_{NB} = 1.10 \pm 0.18$ mm and an outgrowth diameter of ${}^{\rho L}d_{NB} = 1.21 \pm 0.12$ mm in the low ShC density, ρ_L. No statistical differences were measured across ShC densities per EBS solutions although all experiments in EBS solutions. However, all experiments in EBS solutions recorded significantly lower cellular outgrowth ($p < 0.01$) than SCE in all NB media irrespective of extracellular ShC density used. The average diameter of all samples at DIV1, after explant isolation and plating in vitro for 1 day to ensure survival was 0.475 ± 0.0122 mm. Normalizing the data by the original DIV1 diameter, the data illustrates an average change in NB explant outgrowth of 305.26% collected over DIV1 to DIV8 of the experiments. EBS data collected over DIV1 to DIV8 of the experiments illustrated an average change 220.43%.

4 | DISCUSSION

Neurodegeneration and injury impair millions of adults, worldwide. Contemporary therapies have explored the regenerative properties of different biological compounds and neural stem cells to restore NS function by targeting neuronal synapses and multicellular junctions (Ashammakhi et al., 2019; Ottoboni et al., 2020). However, the interactions and synergies of such cell-based treatments with the flow of CSF that surrounds the brain and spinal cord remain underexplored. Tissue engineering systems able to model the fluidic and chemical microenvironments of CSF that interface with neural cells, thereby, offer exciting new avenues with which to examine regenerative strategies for NS disorders.

4.1 | Microenvironment of cerebrospinal fluid

The circulation of CSF has been traditionally regarded as irrigation of the CNS, where fluid produced in the ventricles of the brain flows within and around cranial and spinal SAS, and drains through the glymphatic system (Ratner et al., 2017). In this way, convective flow of CSF creates dynamic chemical microenvironments that nourish the CNS and stimulate appropriate physiological responses of cells on the CSF interface, for example, neurons and glia. However, an emerging model suggests that interstitial flow within the CNS parenchyma is an integral part of CSF circulation and re-absorption (Klarica et al., 2014), with recent evidence reporting cellular waste and blood plasma within CSF believed to result from its local fluid exchange with blood and interstitial fluid (Brinker, Stopa, Morrison, & Klinge, 2014). Recent MRI study further illustrated that tissue diffusivities of CNS gray and white matter modulate its interstitial flow (Liu et al., 2018; Ratner et al., 2017), suggesting CSF circulation occurs via mechanisms of CD. The combined effects of CD create highly nonlinear concentration profiles within microfluidic spinal SAS, which significantly distort the spatial concentration gradients produced via diffusion or convection alone.

Transport via CD is well-studied in many physiological systems at the microscale, where nonlinear and transient distributions of chemical gradients aid cell viability, growth, and response to injury. The bridged gLL system used in this study provides an excellent model of the CSF microenvironment because our microfluidic system is able to produce exact chemical profiles over time using both diffusion and convection (Figure 3). The chemical environment generated using CD within our microfluidic system produced a large range of concentration gradients to stimulate behaviors of CSF-interfacing cells. Specifically, transport within the bridged gLL system created a chemical microenvironment with normalized concentration gradients between 0.85 and 0.01 of the inlet concentration, compared to a linear concentration gradient of 0.72 per mm of channel produced solely via diffusion (Figure 4).

4.2 | Replacement solutions for cerebrospinal fluid

While our microfluidic system produces tunable models of CSF-generated chemical environments, in vitro cell responses to exogenous fields therein depend strongly on the extracellular fluid used to represent CSF. Extracellular solutions of specialized cell and explant media contain a complement of glucose, amino acids, vitamins, lipids, inorganic salts, and other factors that artificially maintain pH and osmolality (McGillicuddy, Floris, Albrecht, & Bones, 2018; Price, 2017). However, the concentrations and mixtures of these molecules vary greatly across media and are largely absent from in vivo CSF (Table 1). As per Table 1, EBS was chosen for its biomimetic properties that closely mimic those of in vivo CSF, particularly osmolarity, pH, and glucose concentration. In addition, EBS lacks artificial compounds added to promote in vitro cell survival and culture, such as phenol red, HEPES buffer, and other amino acids and vitamins.

Moreover, the concentrations and mixtures of components in cell media have evolved over time to optimize monolayer culture, which can potentially affect the behaviors of cells introduced via regenerative therapies (Kaneko et al., 2018; Ottoboni et al., 2020). For instance, DMEM is widely used for culture of glia, such as ShC, but contains twice the concentration of amino acids as in vivo CSF, as well as significantly higher glucose concentration and an artificial dosage of buffer ions (Price, 2017). Similarly, NB media used to culture neuronal cells and CNS explants contains low amounts of amino acids and reduced osmolality compared to in vivo CSF (Brewer, 1997). These discrepancies have led to clinical development of more physiologically relevant cell solutions for NS treatments, including physiological saline, lactated Ringer's solution, artcereb, artificial CSF, and EBS (Shiobara 2013; Trissel 2002). We emphasize that experiments of this study have not altered common culture and explant protocols, but rather compared results using current testing methodologies as they are applied using DMEM, NB, and EBS solutions.

EBS is an FDA-approved, sterile, and isotonic solution commonly used for intrathecal administration of immunosuppressants and chemotherapeutic drugs. It was selected for our study, in part, because of its recent surgical applications as a therapeutic diluent for disorders of the meninges, which partially contain CSF and have been implicated in neuromuscular disease and neurodegenerative disorders (Stark et al., 2019, Garcia Molina et al., 2020). Our study used EBS as a CSF diluent of BDNF, a regenerative therapeutic often used for its ability to affect synaptic transmission, plasticity, and growth of the NMJ via ShC signaling (Pena et al., 2019, Singh et al., 2020). Clinical trials have explored BNDF delivery across the blood brain barrier (Bertram, Rauch, Chang, & Lavik, 2010) and have begun to use emerging models of CSF circulation to develop methodologies that increase local BDNF bioavailability via interstitial flow (Kaneko et al., 2018). Engineering systems able to produce local gradients of BDNF feasible via intrathecal CSF injection (Stark et al., 2019, Shimada et al., 2020) will greatly advance our abilities to interrogate cellular behaviors at CSF interfaces for neuro-repair. We note that the transport of extracellular BDNF is comparable within EBS, DMEM, and NB diluent solutions, as per Equations (4) and (5), and the range for osmolarity and pH shown in Table 1 (Craven, 2010).

4.3 | Behaviors of Schwann Cells within CSF replacement solutions

We first examined the effects of titrated EBS solutions on ShC survival, morphology, and proliferation in vitro (Figure 3). Measured changes in ShC shape over time within titrated EBS solutions were seen to mirror the patterns in ShC morphology recorded in culture using conventional DMEM media. Further, nontitrated EBS solutions stimulated ShC morphologies most similar to those measured in DMEM, with high cell elongation as reported in the literature. Similarly, our data illustrate that ShC cultured in EBS solutions reproduced the proliferation patterns measured in DMEM culture medium and exhibited identical survival rates. In all sets of data, nontitrated EBS solutions stimulated cell behaviors that best mimicked those measured within DMEM. These results are significant because they are the first to illustrate that EBS solutions can be used to support in vitro ShC culture. Such applications will help examine the extent to which ShC maintained exclusively in CSF replacement solutions exhibit behaviors more similar to those in vivo to potentially strengthen development of ShC-based therapies.

Subsequent experiments used EBS as a diluent fluid within the bridged gLL device to produce chemoattractive gradient fields of extracellular BDNF (Figure 5). Previous work from our lab and others have shown that ShC migratory responses to BDNF are important to glia- and NMJ-targeted NS therapies (Singh et al., 2020). The data here illustrate that ShC responded chemotactically to BDNF stimuli generated within DMEM or EBS solutions with high similarity. ShC migration exhibited similar net distances in both extracellular solutions for low, medium, and high BDNF concentration gradients, which were three times those measured in control tests (no BDNF). ShC PLs

were comparable within low and medium BNDF gradient fields produced within both solutions, and slightly higher for higher BDNF gradients created within EBS. Moreover, ShC directionality in all gradient fields was statistically insignificant across both solutions. These data reproduced ShC chemotaxis within solutions that more appropriately represent the osmolality, ionic, and molecular composition of in vivo CSF, to support application of CSF replacement fluids as diluents of targeted regenerative factors in tissue engineering study. Future study will utilize a more physiologically representative extracellular matrix from emerging NS bioscaffold materials, as ShC are known to respond to multiple chemical factors and extracellular macromolecules than the single basement membrane of laminin used in this initial work.

Final experiments then examined the ability of EBS solutions to maintain the viability of SCE cultures and support SCE outgrowth. Organotypic explant cultures from rodent spinal cord represent valuable 3D model systems that retain cytoarchitecture, synaptic properties, and resident spinal cord cells to help develop therapies for restored NS function (Musto et al., 2019). SCE cultures of this project were examined for 8 DIV in both conventional NB and EBS solutions (Figure 5). While differences in survival rates were statistically insignificant, the characteristic size of SCE over 8 days was significantly less (45%) in EBS than in NB, as measured via conventional explant outgrowth. Follow-up tests then used both EBS and NB solutions to introduce increasing extracellular concentrations of ShC and measure resulting SCE outgrowth, currently explored for regeneration (Pohland et al., 2015). Results illustrate that ShC grown in NB solutions produced increased SCE outgrowth with increasing ShC extracellular density, while ShC introduced via EBS solutions did not exhibit statistical differences in SCE outgrowth. These results validate that EBS solutions with more appropriate CSF pH, osmolality, and molecular composition are less likely to support cellular behaviors and outgrowth that may be stimulated by cell media containing excess glucose, amino acids, lipids, and other compounds. Further, EBS solutions lack the external factors that may artificially increase outgrowth via interactions with increased concentrations of cell secretions or signaling. We note that the current study is limited by the outgrowth measurements performed in two-dimensional (2D) culture. Future study will incorporate measurement of neurite extension from SCE samples using a 3D culture system, such as emerging spinal organoids, to physiologically approach in vivo testing with animal models.

In summary, results of our study illustrate that cells and explants can be cultured and examined within clinical CSF replacement solutions using microfluidic environments. The adoption of CSF replacements fluids in tissue engineering is a logical progression in the development of cell-based therapies for CNS regeneration. Use of clinical solutions will increase the significance and translation of in vitro and explant study to advance in vivo testing via animal models and clinical trials.

ACKNOWLEDGEMENTS

This work was supported by the National Science Foundation (NSF CBET 0939511 and NSF EEC 1950509) and the New Jersey Commission on Spinal Cord Research (CSCR14IRG005 and CSCR17ERG005).

CONFLICT OF INTEREST

The authors have declared that there are no conflicts of interest.

AUTHOR CONTRIBUTIONS

Richard N. Cliver, Brian Ayers, and Alyssa Brady contributed significantly to the design of the study and acquisition of experimental data. Bonnie L. Firestein contributed essential reagents, tools, and animal specimens. Richard N. Cliver, Bonnie L. Firestein, and Maribel Vazquez drafted the article and revised it critically for key intellectual content. Maribel Vazquez performed the final revision and approval of the manuscript.

ORCID

Bonnie L. Firestein https://orcid.org/0000-0002-1679-3565
Maribel Vazquez https://orcid.org/0000-0002-6184-3103

REFERENCES

Ashammakhi, N., Kim, H. J., Ehsanipour, A., Bierman, R. D., Kaarela, O., Xue, C., … Seidlits, S. K. (2019). Regenerative therapies for spinal cord injury. *Tissue Engineering Part B: Reviews*, *25*(6), 471–491.

Avossa, D., Rosato-Siri, M. D., Mazzarol, F., & Ballerini, L. (2003). Spinal circuits formation: A study of developmentally regulated markers in organotypic cultures of embryonic mouse spinal cord. *Neuroscience*, *122*(2), 391–405.

Bertram, J. P., Rauch, M. F., Chang, K., & Lavik, E. B. (2010). Using polymer chemistry to modulate the delivery of neurotrophic factors from degradable microspheres: Delivery of BDNF. *Pharmaceutical Research*, *27*(1), 82–91.

Brewer, G. J. (1997). Isolation and culture of adult rat hippocampal neurons. *Journal of Neuroscience Methods*, *71*(2), 143–155.

Brewer, G. J., Torricelli, J. R., Evege, E. K., & Price, P. J. (1993). Optimized survival of hippocampal neurons in B27-supplemented Neurobasal, a new serum-free medium combination. *Journal of Neuroscience Research*, *35*(5), 567–576.

Brinker, T., Stopa, E., Morrison, J., & Klinge, P. (2014). A new look at cerebrospinal fluid circulation. *Fluids and Barriers of the CNS*, *11*, 10.

Castelnovo, L. F., Caffino, L., Bonalume, V., Fumagalli, F., Thomas, P., & Magnaghi, V. (2020). Membrane progesterone receptors (mPRs/PAQRs) differently regulate migration, proliferation, and differentiation in rat Schwann cells. *Journal of Molecular Neuroscience*, *70*(3), 433–448.

Cembran, A., Bruggeman, K. F., Williams, R. J., Parish, C. L., & Nisbet, D. R. (2020). Biomimetic materials and their utility in modeling the 3-dimensional neural environment. *Iscience*, *23*(1), 100788.

Chen, Z., Ma, Z., Wang, Y., Li, Y., Lu, H., Fu, S., … Lu, P. H. (2010). Oligodendrocyte-spinal cord explant co-culture: An in vitro model for the study of myelination. *Brain Research*, *1309*, 9–18.

Craven, J. (2010). Cerebrospinal fluid and its circulation. *Neurosurgical Anaesthesia*, *11*(9), 355–356.

Delbaz, A., Chen, M., Jen, F. E., Schulz, B. L., Gorse, A. D., Jennings, M. P., … Ekberg, J. A. K. (2020). Neisseria meningitidis Induces pathology-associated cellular and molecular changes in trigeminal Schwann cells. *Infection and Immunity*, *88*(4).

Farjah, G. H., Dolatkhah, M. A., Pourheidar, B., & Heshmatian, B. (2017). The effect of cerebrospinal fluid in collagen guide channel on Sciatic nerve regeneration in rats. *Turk Neurosurg*, *27*(3), 453–459.

Flores-Munoz, C., Gomez, B., Mery, E., Mujica, P., Gajardo, I., Cordova, C., … Ardiles, A. O. (2020). Acute Pannexin 1 Blockade Mitigates early synaptic plasticity defects in a mouse model of Alzheimer's disease. *Frontiers in Cellular Neuroscience*, *14*, 46.

Garcia Molina, E., & Penas-Prado, M. (2020). Neoplastic meningitis in solid: Updated review of diagnosis, prognosis, therapeutic management, and future directions. *Neurologia*. Jan 18(S0213-4853 (19)), 30141. https://doi.org/10.1016/j.nrl.2019.10.010

Haines, C., & Goodhill, G. J. (2010). Analyzing neurite outgrowth from explants by fitting ellipses. *Journal of Neuroscience Methods*, *187*(1), 52–58.

Hashemi, E., Sadeghi, Y., Aliaghaei, A., Seddighi, A., Piryaei, A., Broujeni, M. E., … Pouriran, R. (2017). Neural differentiation of choroid plexus epithelial cells: Role of human traumatic cerebrospinal fluid. *Neural Regeneration Research*, *12*(1), 84–89.

Ichida, J. K., & Ko, C. P. (2020). Organoids develop motor skills: 3D human neuromuscular junctions. *Cell Stem Cell*, *26*(2), 131–133.

Jessen, K. R., & Mirsky, R. (2016). The repair Schwann cell and its function in regenerating nerves. *The Journal of Physiology*, *594*(13), 3521–3531.

Kaneko, N., & Sawamoto, K. (2018). Go with the flow: Cerebrospinal fluid flow regulates neural stem cell proliferation. *Cell Stem Cell*, *22*(6), 783–784.

Klarica, M., & Oreskovic, D. (2014). Enigma of cerebrospinal fluid dynamics. *Croatian Medical Journal*, *55*(4), 287–290.

Lackington, W. A., Raftery, R. M., & O'Brien, F. J. (2018). In vitro efficacy of a gene-activated nerve guidance conduit incorporating non-viral PEI-pDNA nanoparticles carrying genes encoding for NGF, GDNF and c-Jun. *Acta Biomaterialia*, *75*, 115–128.

Leister, I., Haider, T., Mattiassich, G., Kramer, J. L. K., Linde, L. D., Pajalic, A., … Aigner, L. (2020). Biomarkers in traumatic spinal cord injury-technical and clinical considerations: A systematic review. *Neurorehabilitation and Neural Repair*, *34*(2), 95–110.

Li, X., Zhang, C., Haggerty, A. E., Yan, J., Lan, M., Seu, M., … Mao, H. Q. (2020). The effect of a nanofiber-hydrogel composite on neural tissue repair and regeneration in the contused spinal cord. *Biomaterials*, *245*, 119978.

Liu, S., Lam, M. A., Sial, A., Hemley, S. J., Bilston, L. E., & Stoodley, M. A. (2018). Fluid outflow in the rat spinal cord: The role of perivascular and paravascular pathways. *Fluids and Barriers of the CNS*, *15*(1), 13.

McGillicuddy, N., Floris, P., Albrecht, S., & Bones, J. (2018). Examining the sources of variability in cell culture media used for biopharmaceutical production. *Biotechnology Letters*, *40*(1), 5–21.

Musto, M., Rauti, R., Rodrigues, A. F., Bonechi, E., Ballerini, C., Kostarelos, K., & Ballerini, L. (2019). 3D organotypic spinal cultures: Exploring neuron and neuroglia responses upon prolonged exposure to graphene oxide. *Frontiers in Systems Neuroscience*, *13*, 1.

Natarajan, A., Sethumadhavan, A., & Krishnan, U. M. (2019). Toward building the neuromuscular junction: In vitro models to study Synaptogenesis and neurodegeneration. *ACS Omega*, *4*(7), 12969–12977.

New, P. W., & Biering-Sorensen, F. (2017). Review of the history of non-traumatic spinal cord dysfunction. *Topics in Spinal Cord Injury Rehabilitation*, *23*(4), 285–298.

Oka, K., Yamamoto, M., Nonaka, T., & Tomonaga, M. (1996). The significance of artificial cerebrospinal fluid as perfusate and endoneurosurgery. *Neurosurgery*, *38*(4), 733–736.

Ottoboni, L., von Wunster, B., & Martino, G. (2020). Therapeutic plasticity of neural stem cells. *Frontiers in Neurology*, *11*, 148.

Pena, J. S., Robles, D., Zhang, S., & Vazquez, M. (2019). A milled microdevice to advance glia-mediated therapies in the adult nervous system. *Micromachines*, *10*(8).

Pohland, M., Glumm, R., Stoenica, L., Holtje, M., Kiwit, J., Ahnert-Hilger, G., … Glumm, J. (2015). Studying axonal outgrowth and regeneration of the corticospinal tract in organotypic slice cultures. *Journal of Neurotrauma*, *32*(19), 1465–1477.

Price, P. J. (2017). Best practices for media selection for mammalian cells. *In Vitro Cellular & Developmental Biology Animal*, *53*(8), 673–681.

Ratner, V., Gao, Y., Lee, H., Elkin, R., Nedergaard, M., Benveniste, H., & Tannenbaum, A. (2017). Cerebrospinal and interstitial fluid transport via the glymphatic pathway modeled by optimal mass transport. *Neuroimage*, *152*, 530–537.

Sasagasako, N., Toda, K., Hollis, M., & Quarles, R. H. (1996). Myelin gene expression in immortalized Schwann cells: Relationship to cell density and proliferation. *Journal of Neurochemistry*, *66*(4), 1432–1439.

Shanmukha, S., Narayanappa, G., Nalini, A., Alladi, P. A., & Raju, T. R. (2018). Sporadic amyotrophic lateral sclerosis (SALS) - skeletal muscle response to cerebrospinal fluid from SALS patients in a rat model. *Disease Models & Mechanisms*, *11*(4).

Shen, M., Tang, W., Cao, Z., Cao, X., & Ding, F. (2017). Isolation of rat Schwann cells based on cell sorting. *Molecular Medicine Reports*, *16*(2), 1747–1752.

Shestakova, A., Healey, J., Zhao, S., Rezk, S., & Nakagiri, J. (2019). Three cases of chronic lymphocytic leukemia/small lymphocytic lymphoma (CLL/SLL) Involving cerebrospinal fluid (CSF). *American Journal of Clinical Pathology*, *152*(Supplement_1), S111–S112.

Shimada, K., Yamaguchi, M., Atsuta, Y., Matsue, K., Sato, K., Kusumoto, S., … Kinoshita, T. (2020). Rituximab, cyclophosphamide, doxorubicin, vincristine, and prednisolone combined with high-dose methotrexate plus intrathecal chemotherapy for newly diagnosed intravascular large B-cell lymphoma (PRIMEUR-IVL): A multicentre, single-arm, phase 2 trial. *The Lancet Oncology*, *21*(4), 593–602.

Shiobara, R., Ohira, T., Doi, K., Nishimura, M., & Kawase, T. (2013). Development of artificial cerebrospinal fluid: Basic experiments, and phase II and III clinical trials. *Journal of Neurology & Neurophysiology*, *4*(5), 1–9.

Singh, T., Robles, D., & Vazquez, M. (2020). Neuronal substrates alter the migratory responses of nonmyelinating Schwann cells to controlled brain-derived neurotrophic factor gradients. *Journal of Tissue Engineering and Regenerative Medicine*, *14*(4), 609–621.

Singh, T., & Vazquez, M. (2019). Time-dependent addition of neuronal and Schwann cells increase myotube viability and length in an in vitro tri-culture model of the neuromuscular junction. *Regenerative Engineering and Translational Medicine*, *5*(4), 402–413.

Sohn, E. J., Jo, Y. R., & Park, H. T. (2019). Downregulation MIWI-piRNA regulates the migration of Schwann cells in peripheral nerve injury. *Biochemical and Biophysical Research Communications*, *519*(3), 605–612.

Stark, J. W., Josephs, L., Dulak, D., Clague, M., & Sadiq, S. A. (2019). Safety of long-term intrathecal methotrexate in progressive forms of MS. *Therapeutic Advances in Neurological Disorders*, *12*, 1–8.

Sun, Z., Worden, M., Wroczynskyj, Y., Yathindranath, V., van Lierop, J., Hegmann, T., & Miller, D. W. (2014). Magnetic field enhanced convective diffusion of iron oxide nanoparticles in an osmotically disrupted cell culture model of the blood-brain barrier. *International Journal of Nanomedicine*, *9*, 3013–3026.

Thomas, J. H. (2019). Fluid dynamics of cerebrospinal fluid flow in perivascular spaces. *Journal of The Royal Society Interface*, *16*(159), 20190572.

Thomson, C. E., Hunter, A. M., Griffiths, I. R., Edgar, J. M., & McCulloch, M. C. (2006). Murine spinal cord explants: A model for evaluating axonal growth and myelination in vitro. *Journal of Neuroscience Research*, *84*(8), 1703–1715.

Thomson, C. E., McCulloch, M., Sorenson, A., Barnett, S. C., Seed, B. V., Griffiths, I. R., & McLaughlin, M. (2008). Myelinated, synapsing cultures of murine spinal cord--validation as an in vitro model of the central nervous system. *European Journal of Neuroscience*, *28*(8), 1518–1535.

Toda, K., Small, J. A., Goda, S., & Quarles, R. H. (1994). Biochemical and cellular properties of three immortalized Schwann cell lines expressing different levels of the myelin-associated glycoprotein. *Journal of Neurochemistry*, *63*(5), 1646–1657.

Trissel, L. A., King, K. M., Zhang, Y., & Wood, A. M. (2002). Physical and chemical stability of methotrexate, cytarabine, and hydrocortisone in Elliott's B Solution for intrathecal use. *Journal of Oncology Pharmacy Practice*, *8*(1), 27–32.

Tsintou, M., Dalamagkas, K., & Makris, N. (2020). Taking central nervous system regenerative therapies to the clinic: Curing rodents versus nonhuman primates versus humans. *Neural Regeneration Researc*, *15*(3), 425–437.

How to cite this article: Cliver RN, Ayers B, Brady A, Firestein BL, Vazquez M. Cerebrospinal fluid replacement solutions promote neuroglia migratory behaviors and spinal explant outgrowth in microfluidic culture. *J Tissue Eng Regen Med*. 2021;15:176–188. https://doi.org/10.1002/term.3164